Pergamon

Journal of Structural Geology, Vol. 18, Nos 2/3, pp. 373 to 383, 1996

0191-8141/96 $15.00+0.00

0191-8141(96)00117-4

Fault-length statistics and implications of graben sets at Candor Mensa, Mars

RICHARD A. SCHULTZ and ANDREA N. FORI

Geomechanics–Rock Fracture Group, Department of Geological Sciences, Mackay School of Mines, University of Nevada, Reno, NV 89557, U.S.A.

(*Received* 8 *January* 1995; *accepted in revised form* 21 *August* 1995)

Abstract—The lengths of individual Martian grabens from three spatially and temporally distinct regional sets are analyzed by a two-dimensional window-sampling method. Length distributions are influenced by fault growth and coalescence processes, image resolution, window size and the post-faulting geologic history of the region. Cumulative length–frequency distributions can be linear for graben lengths between ~30 and 100 km, with slopes (on the area plot) of −2, suggesting self-similar growth of the graben array. Post-faulting geologic processes contribute to concave cumulative-length distributions on the log–log plot, with curtailment and truncation biases producing strongly non-linear distributions for smaller and longer lengths, respectively. Recent evidence for a positive correlation between stratigraphic throw and graben length from analogous terrestrial grabens implies that the magnitudes of throw and extensional strain may also be dependent on relative position along the Martian grabens.

INTRODUCTION

Statistical characterization of fracture populations is becoming an increasingly important tool in studies of jointed and faulted regions (e.g. see relevant sections in Scholz 1990 and Engelder *et al.* 1993). Distributions of fracture lengths, combined with quantitative relationships between length and displacement (e.g. Segall & Pollard 1983, Cowie & Scholz 1992, Walsh & Watterson 1992, Westaway 1994), can provide estimates of strain across a fractured region (e.g. Scholz & Cowie 1990, Marrett & Allmendinger 1991, Walsh *et al.* 1991). Examination of displacement vs length plots can, in principle, identify mechanical layering (e.g. seismogenic depth) as inflections in length and displacement systematics (Scholz *et al.* 1993, Westaway 1994), similar to seismic moment (Scholz 1982, Shimazaki 1986) that also scales with fault size. Thus 'small' faults can be distinguished from 'large' faults given the presence of a layer having appropriate properties and boundary conditions. Fracture populations are known to strongly influence, or control, the strength and deformability of rock masses (e.g. Barton 1976, Hoek & Brown 1980, Priest & Hudson 1981, Rouleau & Gale 1985).

In this paper we report and discuss preliminary measurements of grabens developed in basaltic rocks on Mars. This work is the first phase of a larger effort to remap and interpret the complex faulting history of the Valles Marineris equatorial rift system; Valles Marineris is similar in many respects to terrestrial continental rifts such as the East African (e.g. Ebinger 1989). The grabens are typical of those found on the surfaces of most planets and satellites, with vertical throws of about 100–500 m, widths of 1–3 km, and lengths from 1 to >100 km. They differ, however, in having comparatively straight, linear walls instead of sinuous traces common for terrestrial normal faults (e.g. Bruhn *et al.* 1990, de Polo *et al.* 1991). Stratigraphic offsets across both graben-bounding normal faults appear nearly comparable at the surface (e.g. Davis & Golombek 1990, Chadwick & Lucchitta 1993). Graben depths, estimated from a postulated symmetric, triangular cross-sectional geometry (e.g. Golombek 1979) and plausible dip angles (50–70°) to be 1–5 km, have been interpreted to be indicative, or even diagnostic, of mechanically significant layering (e.g. Golombek 1979, Davis & Golombek 1990). The grabens are unusual given that throws are considered in the literature to be relatively constant with position along the graben for a wide range of graben lengths (from 10 up to 1000 km), although throws can be observed to decrease to zero, as do some graben widths, close to many well-resolved graben terminations.

We focus here on fault-length statistics obtained from three successively younger sets of grabens from the Candor Mensa plateau of Mars. Fault-population statistics are documented and interpreted using both histograms and log–log plots of cumulative length vs frequency. In common with previous work (e.g. Jackson & Sanderson 1992, Gillespie *et al.* 1993), we note challenges in preparing and interpreting these diagrams (e.g. curtailment, truncation and comparison between regions having different counting areas) and plausible solutions. Lastly we apply scaling relationships between displacement and graben length to compare the data from Mars with other data sets obtained from appropriate locations on Earth. Our results are important given current efforts to quantify extensional strains on planets such as Mars (e.g. Plescia 1991, Golombek *et al.* 1994, Tanaka & Chadwick 1994) and to estimate current levels of seismicity (Golombek *et al.* 1992) in preparation for design and emplacement of seismometer arrays on the planet. Because high-quality imaging and (in some

cases) topographic data exist for a variety of planets and satellites (e.g. Greeley 1994) that exhibit relatively uneroded fault sets, interplanetary comparisons of fault-population characteristics will promote a more comprehensive understanding of scaling relationships and fault mechanics (Schultz 1989a). This paper is the first to apply scaling relationships between throw and strike-length, and fault-population statistics, to fractures on another planet.

STUDY AREA AND PREVIOUS WORK

This study builds on an extensive body of literature in planetary structural geology. Decades of research using fly-by, orbital, and lander photographs and digital images of the terrestrial planets, including Mercury, Venus, Moon and Mars, along with more than a dozen icy satellites of the outer planets, such as Ganymede, Callisto, Tethys and Miranda (e.g. Schenk 1991, Lewis 1995), have firmly established that faulting is a fundamental and common process throughout the solar system. The research rests on established principles of image interpretation and structural geomorphology; as a result, unequivocal evidence for normal faulting, thrust faulting and, locally, strike-slip faulting (Schultz 1989a) can be demonstrated for Mars (see review by Banerdt *et al.* 1992). In addition, with little or no liquid water at the surface and a thin atmosphere, erosion and deposition processes that can degrade fault scarps are extremely slow, promoting well-preserved landforms over geologic timescales and facilitating the recognition and interpretation of these nearly pristine landforms in the orbital images.

The plateau grabens accommodate extensional strain in the upper few km of the Candor Mensa region of Mars (Fig. 1), located within the vast Valles Marineris rift

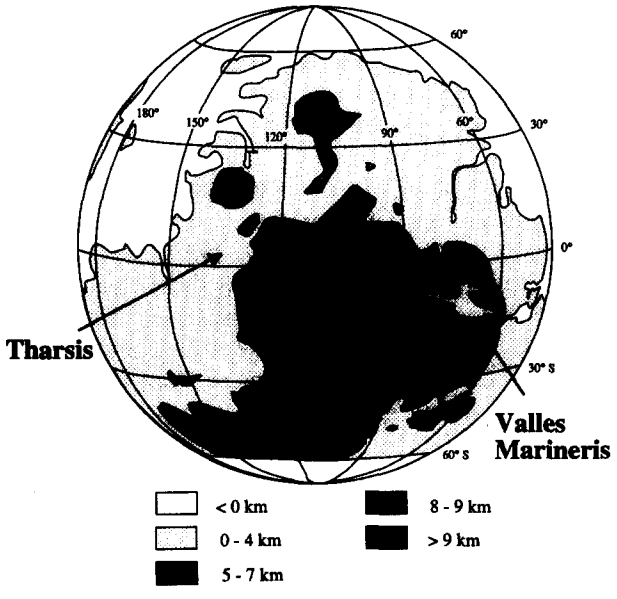

Fig. 1. Location map showing Valles Marineris in relation to major volcanoes in the Tharsis province; regional elevations above Martian reference level given in km. Box shows location of Fig. 2.

system that spans ~3000 km along the Martian equator (see Lucchitta *et al.* 1992 for a geologic and structural overview of the system). The shallow grabens are considerably smaller than the main grabens of the rift system, which have lengths exceeding 1000 km, widths of tens of km and throws of 3–10 km (Schultz 1991). The shallow grabens may comprise the 'small fault' part (Marrett & Allmendinger 1992) of a larger population that includes the main grabens because both classes of grabens appear related spatially and by relative age (e.g. Schultz 1991). The present paper documents statistical characteristics of a particular sample of the 'small' grabens, from a relatively small test area (Fig. 2), extracted from the total fault population.

Earth and Mars have important differences, as well as useful similarities, that bear on comparisons of faulting and population statistics from both planets. More than half of the Martian surface is covered by basaltic lava flows (Greeley & Spudis 1981) that emanated from either volcanoes or fissure vents; the grabens discussed in this paper were formed on a basaltic plateau 3–3.5 Ga ago (Upper Hesperian time; see Tanaka 1986 for discussion of the Martian geologic time scale and correlations with absolute ages). The surface gravity of Mars, 3.7 m s^{-2}, is only 38% that of Earth. Assuming comparable rock densities of 2900 kg m^{-3} (for intact basalt), overburden stress at any given depth on Mars will be 38% of that for the same depth on Earth. In addition, the low surface temperature at the Martian equator, <0°C, plausible ranges of geothermal gradient and minuscule atmospheric pressure (6 mbar) imply that the crust is frozen and/or desiccated to depths of several km (e.g. Clifford 1993) so that pore-water pressure near the fault zones is negligibly small. The frictional strength of Martian basalts is probably comparable to that of terrestrial basalts (e.g. Byerlee 1978, Schultz 1995) for conditions of low confining pressure, low temperature and weathered rock surfaces.

The study area (Fig. 2) is composed of two main physiographic regions (Lucchitta & Schultz unpublished map): plateau and trough (defined by depressions up to 5 km deep and formed by tectonic and erosional processes; see Fig. 3). At least three generations (or sets) of normal faults were formed on the plateau, including an E–W-trending set, a N–S-trending set, and the oldest NE-trending set (Fig. 3a). Each set is distinct in orientation and in relative age, based on clear cross-cutting relationships (Fig. 3b), implying temporally variable stress trajectories in this region. The main, large grabens comprising the large Valles Marineris troughs (Blasius *et al.* 1977, Schultz 1991, Lucchitta *et al.* 1994) may be contemporaneous with the E–W-trending set. Troughs and impact craters were formed after graben faulting on the plateau, leading to overprinting and curtailment (Priest 1993) of fault lengths.

Symmetric grabens can form above dikes as a result of near-tip stresses interacting with the free surface (e.g. Pollard *et al.* 1983, Mastin & Pollard 1988, Rubin & Pollard 1988), and Schultz (1989b) and Tanaka *et al.* (1991) among others hypothesized that some Martian

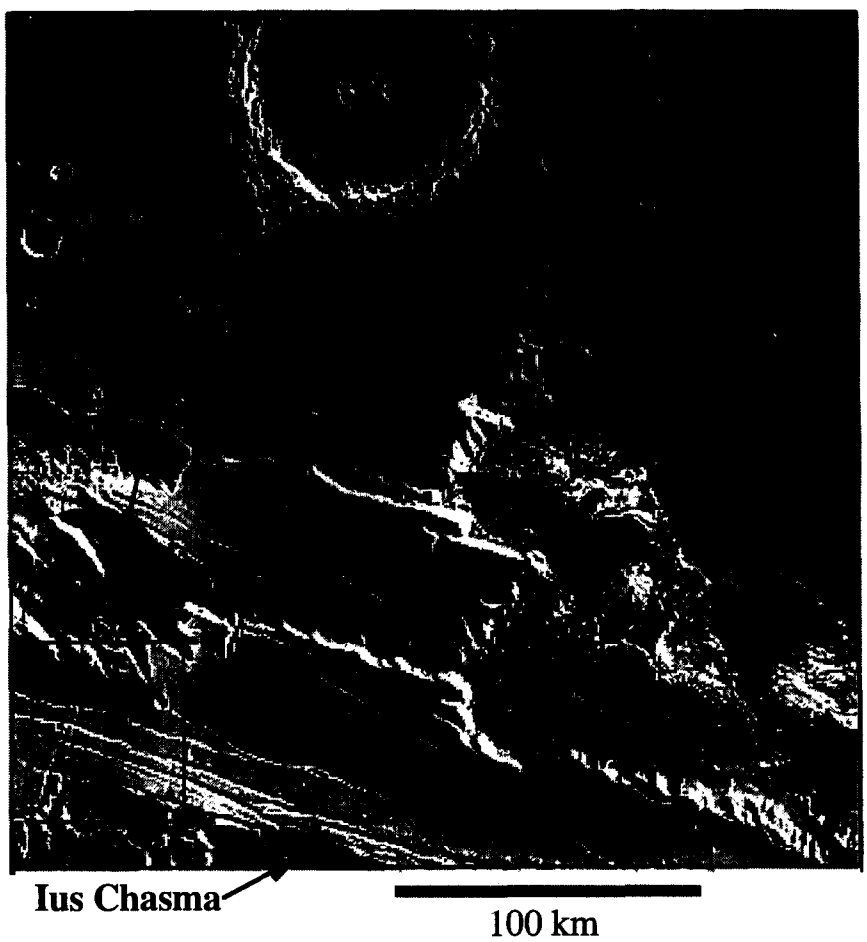

Fig. 2. Digital image mosaic of Candor Mensa region of Mars showing multiple graben sets developed on plateau. Note large impact crater Perrotin at top (~70 km diameter) and depressions such as Candor Chasma ('troughs' formed by tectonic subsidence and erosion) that cover or destroy previously formed graben sets. Elevation change from plateau to floor of troughs 1–3 km; typical image resolution ~250 m pixel $^{-1}$. Inset shows location of Fig. 3(a). Data obtained from Mars Digital Image Map CD-ROM, Vol. 2: Xanthe Terra, MTM -5077 quadrangle, available from U.S. Geological Survey, Flagstaff, Arizona, U.S.A. (khoyt@astrog.span.nasa.gov).

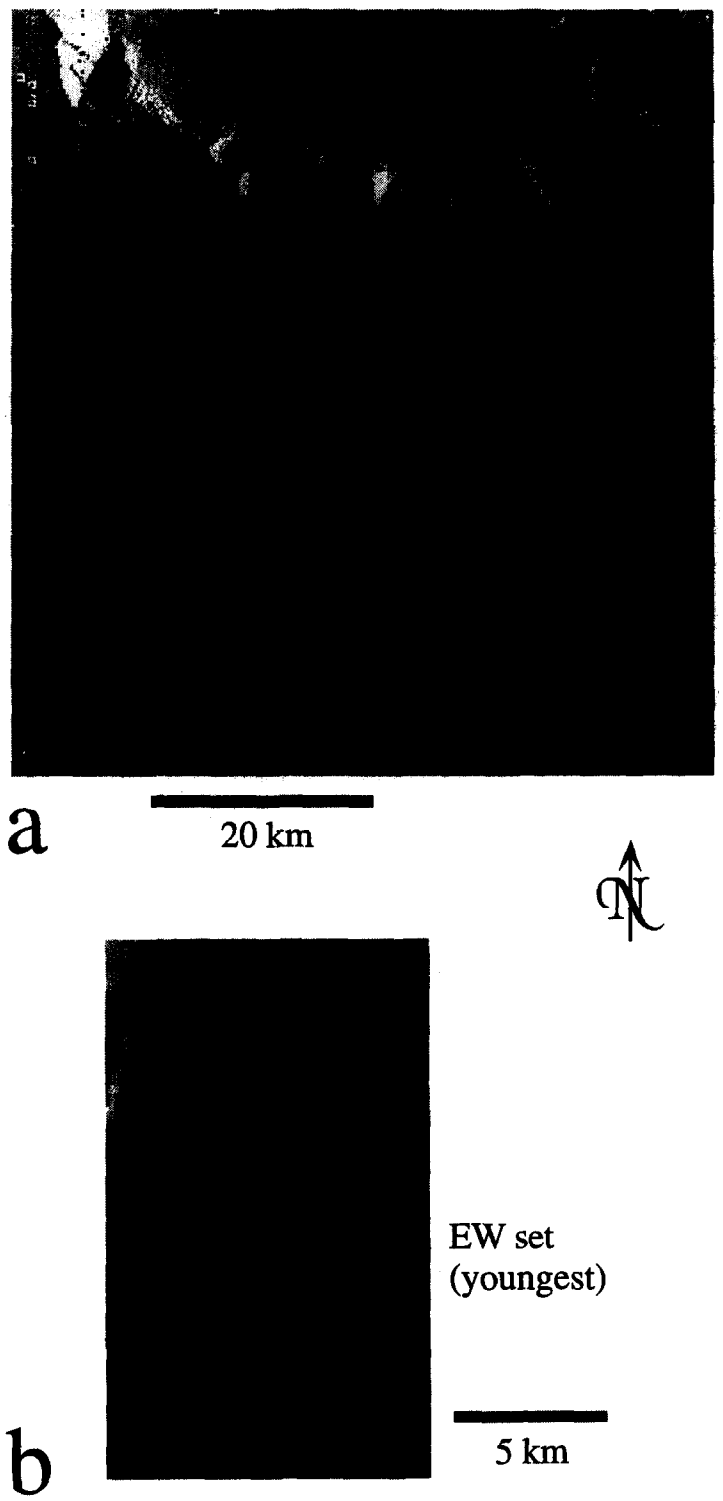

Fig. 3. Enlargements of image 920A14 showing (a) graben sets (trends aligned with arrows) and (b) cross-cutting relations demonstrating that E–W grabens are younger than N–S grabens.

grabens could overlie dikes. The depths of these grabens would be limited by the depth to dike tops, which is controlled by magma pressure and other factors (e.g. Rubin 1990, 1995). Graben lengths would be controlled by the horizontal extent of the dikes, which is influenced by remote stress and magma pressure. Although some Martian and lunar grabens possess central fissure vents and other features characteristic of such 'volcanic' grabens (Head & Wilson 1993), those at Candor Mensa do not. While we can not definitively preclude a volcanic origin for the dikes at Candor Mensa, the lack of supporting evidence such as central fissures or flows suggests to us that the grabens are associated with regional extensional strain in which dike injection was at best a small component. Many previous workers have also inferred that the plateau grabens are tectonic, related to localized extension and perhaps rifting at Valles Marineris (e.g. Lucchitta *et al.* 1992), rather than volcanic.

DATA AND METHODS

A two-dimensional window-sampling technique (Pahl 1981) is used to count fault lengths on the plateau. All grabens within the region (Fig. 2) were recorded; data include length, orientation, linkage with other faults/grabens and nature of terminations. Most grabens either dissect or transect the window (e.g. Priest 1993, p. 46) in the sense that lengths are indeterminate due to overprinting of craters, their ejecta blankets and the large troughs. However, many structures are fully contained within the window. The curtailment bias due to these uncertainties in identifying graben length is apparent in the log–log plots discussed below. We attempted to adjust for curtailment bias by connecting collinear grabens, partially covered by later materials, to provide an estimate of the original fault-length distributions for each set of grabens (the 'interpreted' data, see Table A2). Few grabens <1 km long were recorded as this value is comparable to the uncertainty in locating fault terminations precisely on the medium resolution (~250 m pixel^{-1}) images. Truncation bias due to undersampling of the shorter grabens is also apparent in the fault-population statistics. Both of these effects contribute to a more random appearing, non-power-law distribution of graben lengths in the region.

Larger grabens on the plateau apparently grew by coalescence of smaller faults, as suggested by echelon or irregular fault segments preserved along both opposing fault walls (e.g. Fig. 3b). Grabens were counted as single entities where they clearly cross-cut other structures or terminate, regardless of fault-wall structure. Grabens that merge at shallow angles into other grabens were identified as separate structures when their length beyond the graben exceeded that graben's width. Our approach produces fault-length statistics for the final fault geometry and does not explicitly include the many smaller faults that were incorporated into the counted structures.

The fault-length data (Tables A1 and A2 of the Appendix) were converted to log–log plots of cumulative frequency vs graben length (Fig. 5) that allow comparisons of different data sets from regions of arbitrary measurement area. The cumulative number of faults having lengths $\geq L$ is first scaled to a reference area, following established conventions (Crater Analysis Techniques Working Group 1979, Jackson & Sanderson 1992). Although some workers normalize their plots to a standard traverse length or area (e.g. Jackson & Sanderson 1992, Scholz *et al.* 1993), most do not. Instead of using a small, 1 km^2 reference area (or a 1 km reference length for line surveys), we define a reference area of 100 × 100 km (10^4 km^2), large enough to aid in comparing our results to those obtained from other large regions. Error bars (Crater Analysis Techniques Working Group 1979, appendix) calculated for each length value decrease with increasing cumulative number, reflecting systematic differences in the number of points being represented at each length value on the diagram.

RESULTS AND DISCUSSION

Histograms showing the relative frequency of graben lengths in each of the three age sets (Fig. 4) illustrate differences between the sets. For example, the relative paucity of longer grabens ($L > \sim 80$ km) in the oldest, NE-trending set may reflect partial infilling by later deposits (e.g. Fig. 3b) or perhaps insufficient strain to promote the growth of longer faults. Attempts to fit each histogram with a single ideal probability distribution function (random, power law) were unsuccessful. This result may not be too surprising given the relatively small number of counted faults as well as other factors that can contribute to the length systematics including self-similar growth of faults, fault interaction and graben formation, and the randomizing effects of geologic overprinting and related truncations biases, as well as the fixed size of the counting window (total area of image mosaic, Fig. 2). Some of these effects were modeled by Gillespie *et al.* (1993), who noted that certain characteristics that are scale-invariant can be masked in length–frequency plots. Adjustment for curtailment bias produced a reduction in the number of shorter grabens and a corresponding increase in the number of longer grabens (Fig. 4, unfilled bars).

Cumulative-frequency diagrams (Fig. 5) show that the lengths of plateau grabens may follow a power-law distribution (linear slope) within a particular length band. For example, graben lengths for all three sets could be approximated by a −2 slope for lengths greater than 20–30 km. However, the effects of undersampling at small lengths, and those of curtailment bias at large lengths, are clearly evident. Fall-off of the data to shallower slopes at small lengths (<20–30 km) due to undersampling (and image resolution) is well known in both the fault-statistics and crater-statistics literature. The corresponding steepening at large lengths results from curtailment bias (e.g. Jackson & Sanderson 1992).

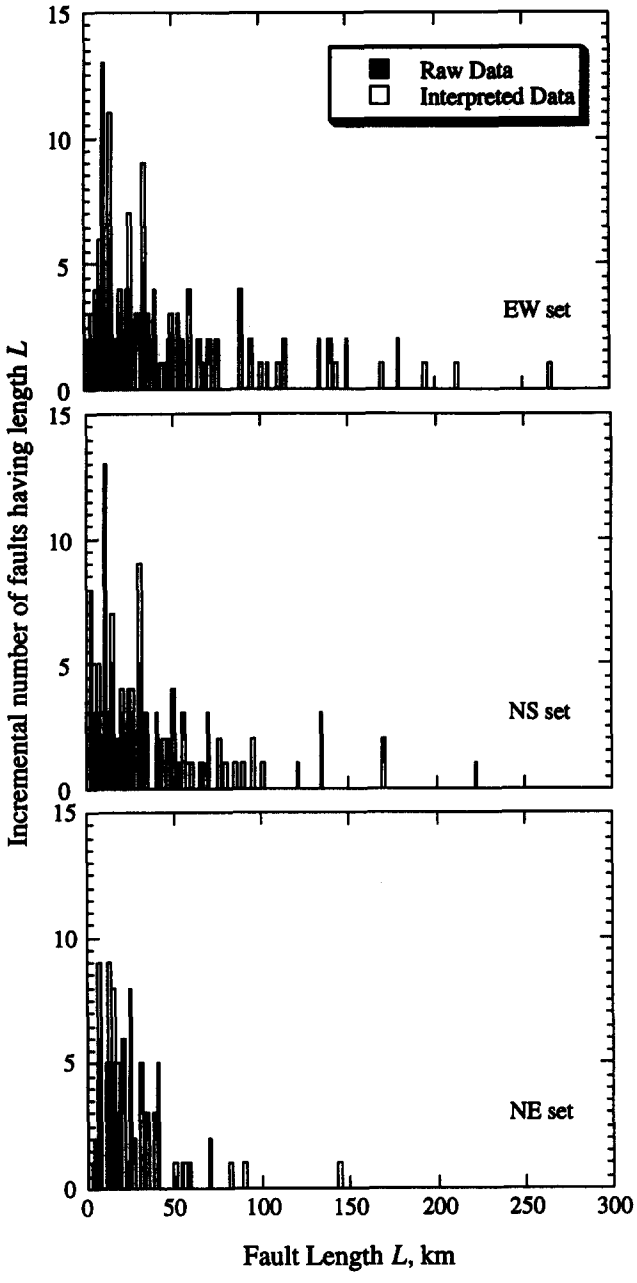

Fig. 4. Histograms showing graben lengths in each set; E–W set, top, is youngest; NE set, bottom, is oldest. Filled bars represent measured lengths of grabens: unfilled bars represent the interpreted data adjusted for curtailment bias.

Correction for curtailment and overprinting biases (Fig. 5, unfilled symbols) shifts the points to the right toward greater lengths, along with a small reduction in the total number of faults (see Table A2). The error bars on the plots illustrate the typical ambiguities associated with fitting slopes from small cumulative lengths, whose larger numbers imply smaller uncertainties, to large cumulative lengths that may or may not fully occur within the sampling window. Formal presentation of statistical uncertainties is critical to an accurate assessment of slope changes and corresponding inferences of cross-over points (Cowie & Scholz 1992) between small and large faults (e.g. Scholz 1982).

According to previous investigations of Martian fault sets, graben throws are not considered to vary systemati-

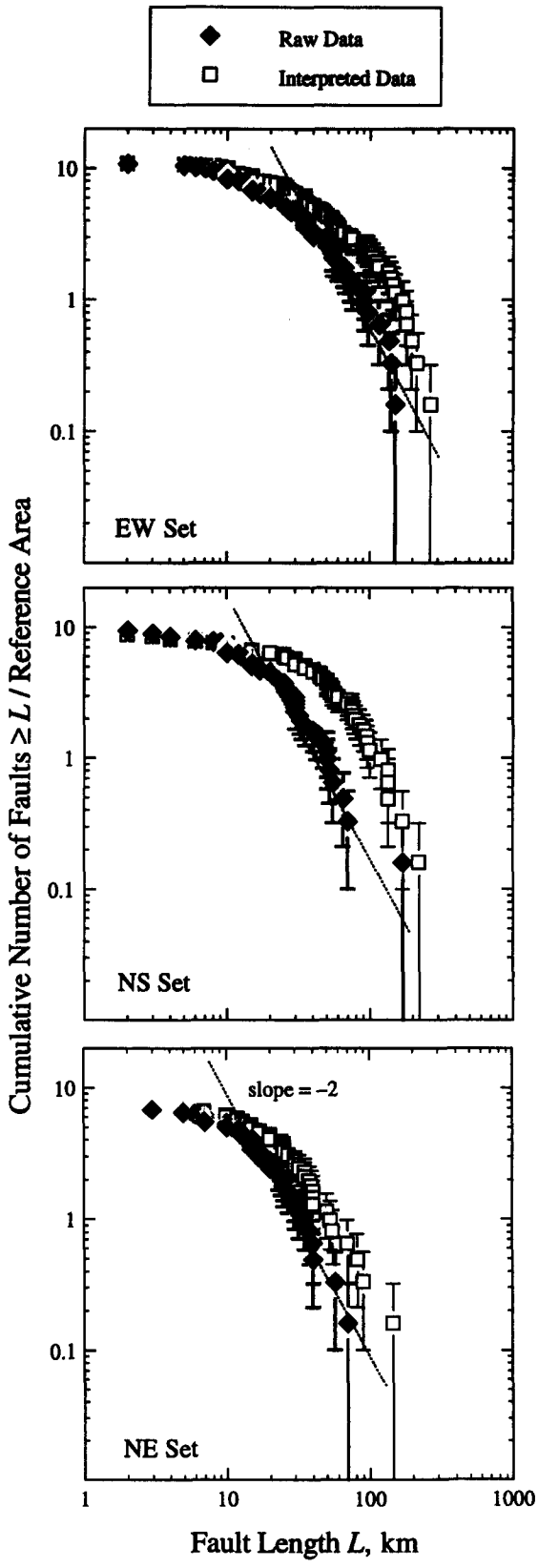

Fig. 5. Cumulative number of grabens, normalized by reference area (10^4 km^2) vs length. Calculated uncertainties due to population statistics (error bars in figure) are listed in the Appendix. Filled and unfilled symbols as in Fig. 4. Dotted lines show slope for self-similar (fractal) distribution (slope of −2 for area plot, Jackson & Sanderson 1992) for illustration, not as quantitative fit to data range.

cally with graben length (e.g. Golombek 1979, Davis & Golombek 1990, Plescia 1991). Indeed, many planetary geologists assume that throw and extensional strain are constant along the entire length of a lunar or Martian graben. Measurements of throw T and length L from normal faults in basalt from Earth (the Krafla fissure set, Opheim & Gudmundsson 1989) and Mars (Davis & Golombek 1990) are plotted in Fig. 6 along with plausible ratios of T/L from Cowie & Scholz (1992). T/L data from the grabens from Canyonlands National Park, Utah (Trudgill & Cartwright 1994, Cartwright *et al.* 1995) are also included as a comparable terrestrial analog to the Martian grabens (McGill & Stromquist 1979), rock type differences (sandstone vs basalt) notwithstanding. Throws along both the Krafla faults and Canyonlands grabens clearly scale proportionally with strike-length. Although topographic data for the Candor Mensa grabens are not presently sufficient to resolve the relationship between throw and graben length for these shallow structures, preliminary measurements (Fori unpublished data 1995) along the large trough grabens such as Coprates Chasma (Schultz 1991) demonstrate that throw varies systematically with position along these large Martian grabens, similar to relationships found for the Canyonlands grabens on Earth. We hypothesize that the Candor Mensa grabens also follow an analogous scaling law between throw and strike-length; forthcoming high-resolution topographic data from the Mars Global Surveyor spacecraft can be used to test this critical hypothesis for the smaller plateau grabens.

Regional strain estimates obtained from single measurements of throw across multiple grabens (without reference to the relative position along the structure) on Mars and the Moon (e.g. Plescia 1991, Golombek *et al.* 1994, Tanaka & Chadwick 1994) have assumed that throw is independent of strike-length. These values may require some revision if the uncertainty in calculated throw for the Martian and lunar examples is less than the variation in throw with position along the graben. Because throws along terrestrial grabens are proportional to graben lengths, the predictions of present-day seismicity, obtained in part from the length distribution of small grabens (Golombek *et al.* 1992) comparable to those presented in this paper, now have a stronger physical basis.

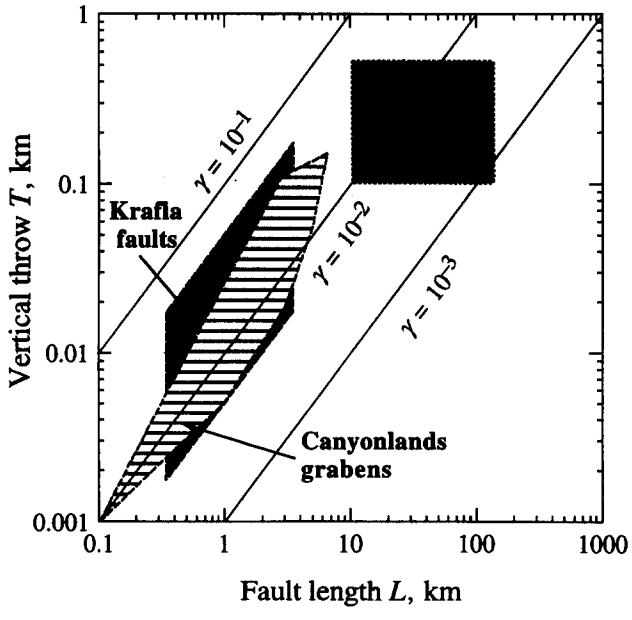

Fig. 6. Comparison of vertical throw vs fault length data from Earth and Mars. Krafla fault data (shaded) bounded by $T = 0.05L$ and $T = 0.005L$ (Opheim & Gudmundsson 1989); range of Canyonlands graben data (Cartwright *et al.* 1995) shown by hatchured shape; Mars bound estimated from inferred throws of 100–500 m along grabens ranging from 10 to 200 km long. Lines of constant shear strain near fault tips (Cowie & Scholz 1992) shown for plausible range of values for $\gamma = T/L$.

Some previous workers (e.g. Davis & Golombek 1990) have hypothesized that stratigraphic or compositional variations can control graben nucleation and depth, implying that graben length–frequency statistics could be used to 'map out' mechanically important layers. For example, a statistically significant change in slope on the log–log plots near fault lengths comparable to, or twice, the layer thickness (e.g. Dawers *et al.* 1993, Scholz *et al.* 1993) could be interpreted as a temperature-controlled transition from small to seismogenically large faults (Scholz 1982). We find no support in the cumulative length–frequency plots (Fig. 5) for mechanically significant layering, or frictional stability transitions (Tse & Rice 1986), at depth in the Candor Mensa area, even for graben lengths of about 100 km. Dawers *et al.* (1993) counted fault lengths from a 150-thick layer of welded tuff from California. They also were unable to resolve a break in slope for the cumulative length–frequency data (reported by Scholz *et al.* 1993), perhaps suggesting that not enough strain had accumulated for significant changes in length systematics to become noticeable (Dawers personal communication 1994) or that the faults penetrated through the tuff without greatly changing their statistical characteristics. We infer that modest lithologic and/or compositional changes oriented at high angles to faults (cf. Wojtal 1994) may not be easily resolved by log–log plots of cumulative length data.

CONCLUSIONS

Fault populations from a plateau on Mars are analyzed statistically and compared to those from Earth. Biases affect both the short and long ends of the fault-length distributions obtained from the window sampling scheme; these biases arise from window size and, more importantly, from modifications of fault-length statistics by later, post-faulting geologic processes. In spite of these complexities, power-law (fractal) distributions of graben lengths are permitted by the data for all three faults sets examined. Given available measurements of terrestrial grabens which demonstrate that throw scales proportionally with strike-length, we infer that the Martian grabens also follow normal throw–strike-length scaling relationships.

Acknowledgements—Reviews by Ian Main and two anonymous referees significantly improved the paper. This work was supported by NASA Planetary Geology and Geophysics Program grant NAGW-4151 to R. A. Schultz.

REFERENCES

Banerdt, W. B., Golombek, M. P. & Tanaka, K. L. 1992. Stress and tectonics on Mars. In: *Mars* (edited by Kieffer, H. H., Jakosky, B. M., Synder, C. W. & Matthews, M. S.). University of Arizona Press, Tueson, 249–297.

Barton, N. 1976. The shear strength of rock and rock joints. *Int. J. Rock Mech. Min. Sci. & Geomech. Abs.* **13**, 255–279.

Blasius, K. R., Cutts, J. A., Guest, J. E. & Masursky, H. 1977. Geology of the Valles Marineris: First results of imaging from the Viking 1 Orbiter primary mission. *J. geophys. Res.* **82**, 4067–4091.

Bruhn, R. L., Yonkee, W. A. & Parry, W. T. 1990. Structural and fluid-chemical properties of seismogenic normal faults. *Tectonophysics* **175**, 139–157.

Byerlee, J. 1978. Friction of rocks. *Pure & Appl. Geophys.* **116**, 615–626.

Cartwright, J. A., Trudgill, B. D. & Mansfield, C. S. 1995. Fault growth by segment linkage: an explanation for scatter in maximum displacement and trace length data from the Canyonlands Grabens of SE Utah. *J. Struct. Geol.* **17**, 1319–1326.

Chadwick, D. J. & Lucchitta, B. K. 1993. Fault geometries and extension in the Valles Marineris, Mars. (Abs.) *Lunar Planet. Sci.* **XXIV**, 263–264.

Clifford, S. M. 1993. A model for the hydrologic and climatic behavior of water on Mars. *J. geophys. Res.* **98**, 10,973–11,016.

Cowie, P. A. & Scholz, C. H. 1992. Displacement-length scaling relationship for faults: data synthesis and discussion. *J. Struct. Geol.* **14**, 1149–1156.

Crater Analysis Techniques Working Group. 1979. Standard techniques for presentation and analysis of crater size–frequency data. *Icarus* **37**, 467–474.

Davis, P. A. & Golombek, M. P. 1990. Discontinuities in the shallow Martian crust at Lunae, Syria, and Sinai Plana. *J. geophys. Res.* **95**, 14,231–14,248.

Dawers, N. H., Anders, M. H. & Scholz, C. H. 1993. Growth of normal faults: Displacement-length scaling. *Geology* **21**, 1107–1110.

dePolo, C. M., Clark, D. G., Slemmons, D. B. & Ramelli, A. R. 1991. Historical surface faulting in the Basin and Range province, western North America: implications for fault segmentation. *J. Struct. Geol.* **13**, 123–136.

Ebinger, C. J. 1989. Geometric and kinematic development of border faults and accommodation zones, Kivu-Rusizi rift, Africa. *Tectonics* **8**, 117–133.

Engelder, T., Fischer, M. P. & Gross, M. R. 1993. Geological aspects of fracture mechanics. *Geol. Soc. Am. Short Course Notes.*

Gillespie, P. A., Howard, C. B., Walsh, J. J. & Watterson, J. 1993. Measurement and characterisation of spatial distributions of fractures. *Tectonophysics* **226**, 113–141.

Golombek, M. P. 1979. Structural analysis of lunar grabens and the shallow crustal structure of the Moon. *J. geophys. Res.* **84**, 4657–4666.

Golombek, M. P., Banerdt, W. B., Tanaka, K. L. & Tralli, D. M. 1992. A prediction of Mars seismicity from surface faulting. *Science* **258**, 979–981.

Golombek, M. P., Tanaka, K. L., Chadwick, D. J., Franklin, B. J. & Davis, P. A. 1994. Extension across Tempe Terra and Sirenum provinces on Mars from measurements of fault scarp widths. (Abs.) *Lunar Planet. Sci.* **XXV**, 443–444.

Greeley, R. 1994. *Planetary Landscapes* (2nd edn). Chapman & Hall, New York.

Greeley, R. & Spudis, P. D. 1981. Volvanism on Mars. *Rev. Geophys.* **19**, 13–41.

Head, J. W., III & Wilson, L. 1993. Lunar graben formation due to near-surface deformation accompanying dike emplacement. *Planet. Space Sci.* **41**, 719–727.

Hoek, E. & Brown, E. T. 1980. Empirical strength criterion for rock masses. *J. Geotech. Div., Am. Soc. Civ. Engrs* **106**, 1013–1035.

Jackson, P. & Sanderson, D. J. 1992. Scaling of fault displacement from the Badajoz–Córdoba shear zone, SW Spain. *Tectonophysics* **210**, 179–190.

Lewis, J. S. 1995. *Physics and Chemistry of the Solar System.* Academic Press, San Diego.

Lucchitta, B. K., McEwen, A. S., Clow, G. D., Geissler, P. E., Singer, R. B., Schultz, R. A. & Squyres, S. W. 1992. The canyon system of Mars. In: *Mars* (edited by Kieffer, H. H., Jakosky, B. M., Snyder, C. W. & Matthews, M. S.). University of Arizona Press, Tucson, 453–492.

Lucchitta, B. K., Isbell, N. K. & Howington-Kraus, A. 1994. Topography of Valles Marineris: Implications for erosional and structural history. *J. geophys. Res.* **99**, 3783–3798.

Marrett, R. & Allmendinger, R. W. 1991. Estimates of strain due to brittle faulting: sampling of fault populations. *J. Struct. Geol.* **13**, 735–738.

Marrett, R. & Allmendinger, R. W. 1992. Amount of extension on "small" faults: An example from the Viking graben. *Geology* **20**, 47–50.

Mastin, L. G. & Pollard, D. D. 1988. Surface deformation and shallow dike intrusion processes at Inyo Craters, Long Valley, California. *J. geophys. Res.* **93**, 13,221–13,235.

McGill, G. E. & Stromquist, A. W. 1979. The grabens of Canyonlands National Park, Utah: Geometry, mechanics, and kinematics. *J. geophys. Res.* **84**, 4547–4563.

Opheim, J. A. & Gudmundsson, A. 1989. Formation and geometry of fractures, and related volcanism, of the Krafla fissure swarm, northeast Iceland. *Bull. geol. Soc. Am.* **101**, 1608–1622.

Pahl, P. J. 1981. Estimating the mean length of discontinuity traces. *Int. J. Rock Mech. Min. Sci. & Geomech. Abs.* **18**, 221–228.

Plescia, J. B. 1991. Graben and extension in northern Tharsis, Mars. *J. geophys. Res.* **96**, 18,883–18,895.

Pollard, D. D., Delaney, P. T., Duffield, W. A., Eno, E. T. & Okamura, A. T. 1983. Surface deformation in volcanic rift zones. *Tectonophysics* **94**, 541–584.

Priest, S. D. 1993. *Discontinuity Analysis for Rock Engineering.* Chapman & Hall, London.

Priest, S. D. & Hudson, J. A. 1981. Estimation of discontinuity spacing and trace length using scanline surveys. *Int. J. Rock Mech. Min. Sci. & Geomech. Abs.* **18**, 183–197.

Rouleau, A. & Gale, J. E. 1985. Statistical characterization of the fracture system in the Stripa Granite, Sweden. *Int. J. Rock Mech. Min. Sci. & Geomech. Abs.* **22**, 353–367.

Rubin, A. M. 1990. A comparison of rift-zone tectonics in Iceland and Hawaii. *Bull. Volcanol.* **52**, 302–319.

Rubin, A. M. 1995. Propagation of magma-filled cracks. *A. Rev. Earth Planet. Sci.* **23**, 287–336.

Rubin, A. M. & Pollard, D. D. 1988. Dike-induced faulting in rift zones of Iceland and Afar. *Geology* **16**, 143–147.

Schenk, P. M. 1991. Outer planet satellites. *Rev. Geophys.* Suppl., 297–305.

Scholz, C. H. 1982. Scaling laws for large earthquakes: Consequences for physical models. *Bull. seism. Soc. Am.* **72**, 1–14.

Scholz, C. H. 1990. *The Mechanics of Earthquakes and Faulting.* Cambridge University Press, New York.

Scholz, C. H. & Cowie, P. A. 1990. Determination of total strain from faulting using slip measurements. *Nature* **346**, 837–838.

Scholz, C. H., Dawers, N. H., Yu, J.-Z. & Anders, M. H. 1993. Fault growth and fault scaling laws: Preliminary results. *J. geophys. Res.* **98**, 21,951–21,961.

Schultz, R. A. 1989a. Strike-slip faulting of ridged plains near Valles Marineris, Mars. *Nature* **341**, 424–426.

Schultz, R. A. 1988b. Do pit-crater chains grow up to be Valles Marineris canyons? (Abs.) *Lunar Planet. Institute Tech. Rep.* **89-06**, 47–48.

Schultz, R. A. 1991. Structural development of Coprates Chasma and western Ophir Planum, central Valles Marineris rift, Mars. *J. geophys. Res.* **96**, 22,777–22,792.

Schultz, R. A. 1995. Limits on strength and deformation properties of jointed basaltic rock masses. *Rock Mech. & Rock Engng* **28**, 1–15.

Segall, P. & Pollard, D. D. 1983. Joint formation in granitic rock of the Sierra Nevada. *Bull. geol. Soc. Am.* **94**, 563–575.

Shimazaki, K. 1986. Small and large earthquakes: The effects of the thickness of seismogenic layer and the free surface. In: *Earthquakes Source Mechanics* (edited by Das, S., Boatwright, J. & Scholz, C. H.). *Am. Geophys. Un. Geophys. Monogr.* **37**, 209–216.

Tanaka, K. L. 1986. The stratigraphy of Mars. *J. geophys. Res.* **91**, E139–E158.

Tanaka, K. L. & Chadwick, D. J. 1994. Extensional history of Mars' Tharsis region. (Abs.) *Lunar Planet. Sci.* **XXV**, 1397–1398.

Tanaka, K. L., Golombek, M. P. & Banerdt, W. B. 1991. Reconciliation of stress and structural histories of the Tharsis region of Mars. *J. geophys. Res.* **96**, 15,617–15,633.

Trudgill, B. & Cartwright, J. 1994. Relay-ramp forms and normal-

fault linkages, Canyonlands National Park, Utah. *Bull. geol. Soc. Am.* **106**, 1143–1157.
Tse, S. T. & Rice, J. R. 1986. Crustal earthquake instability in relation to the depth variation of frictional slip processes. *J. geophys. Res.* **91**, 9452–9472.
Walsh, J. J. & Watterson, J. 1992. Populations of faults and fault displacements and their effects on estimates of fault-related regional extension. *J. Struct. Geol.* **14**, 701–712.
Walsh, J., Watterson, J. & Yielding, G. 1991. The importance of small-scale faulting in regional extension. *Nature* **351**, 391–393.
Westaway, R. 1994. Quantitative analysis of populations of small faults. *J. Struct. Geol.* **16**, 1259–1273.
Wojtal, S. F. 1994. Fault scaling laws and the temporal evolution of fault systems. *J. Struct. Geol.* **16**, 603–612.

APPENDIX

Table A1. Fault-length data (raw)

L (km)	ΣN^*	$\pm 1\,\sigma$	L (km)	ΣN^*	$\pm 1\,\sigma$
E–W set (youngest), $N = 67$			75	1.30	0.46
2	10.89	1.33	90	1.14	0.43
5	10.72	1.32	90	0.98	0.40
5	10.56	1.31	96	0.81	0.36
6	10.40	1.30	115	0.65	0.33
6	10.24	1.29	135	0.49	0.28
7	10.07	1.28	140	0.33	0.23
8	9.91	1.27	150	0.16	0.16
8	9.75	1.26	N–S set, $N = 59$		
8	9.59	1.25	2	9.59	1.25
9	9.42	1.24	2	9.42	1.24
10	9.26	1.23	3	9.26	1.23
10	9.10	1.22	3	9.10	1.22
10	8.94	1.21	3	8.94	1.21
10	8.77	1.19	4	8.77	1.19
10	8.61	1.18	4	8.61	1.18
10	8.45	1.17	4	8.45	1.17
10	8.29	1.16	6	8.29	1.16
12	8.12	1.15	6	8.12	1.15
13	7.96	1.14	6	7.96	1.14
13	7.80	1.13	8	7.8	1.13
14	7.64	1.11	9	7.64	1.11
15	7.47	1.10	10	7.47	1.10
15	7.31	1.09	10	7.31	1.09
15	7.15	1.08	10	7.15	1.08
15	6.99	1.07	10	6.99	1.07
15	6.83	1.05	10	6.83	1.05
17	6.66	1.04	10	6.66	1.04
17	6.50	1.03	10	6.50	1.03
20	6.34	1.01	10	6.34	1.01
20	6.18	1.00	12	6.18	1.00
20	6.01	0.99	13	6.01	0.99
23	5.85	0.98	13	5.85	0.98
25	5.69	0.96	15	5.69	0.96
25	5.53	0.95	15	5.53	0.95
26	5.36	0.93	15	5.36	0.93
26	5.20	0.92	15	5.20	0.92
26	5.04	0.9	15	5.04	0.90
27	4.88	0.89	16	4.88	0.89
28	4.71	0.88	17	4.71	0.88
30	4.55	0.86	20	4.55	0.86
32	4.39	0.84	20	4.39	0.84
35	4.23	0.83	21	4.23	0.83
35	4.06	0.81	22	4.06	0.81
35	3.90	0.80	23	3.90	0.80
35	3.74	0.78	25	3.74	0.78
35	3.58	0.76	25	3.58	0.76
37	3.41	0.74	26	3.41	0.74
40	3.25	0.73	26	3.25	0.73
40	3.09	0.71	27	3.09	0.71
48	2.93	0.69	30	2.93	0.69
50	2.76	0.67	30	2.76	0.67
50	2.60	0.65	30	2.60	0.65
53	2.44	0.63	30	2.44	0.63
54	2.28	0.61	30	2.28	0.61
55	2.11	0.59	32	2.11	0.59
59	1.95	0.56	33	1.95	0.56
65	1.79	0.54	35	1.79	0.54
67	1.63	0.51	40	1.63	0.51
72	1.46	0.49	42	1.46	0.49

Table A1. *Continued*

L (km)	ΣN^*	$\pm 1\,\sigma$	L (km)	ΣN^*	$\pm 1\,\sigma$
47	1.30	0.46	15	4.06	0.81
50	1.14	0.43	15	3.90	0.80
50	0.98	0.40	15	3.74	0.78
52	0.81	0.36	15	3.58	0.76
55	0.65	0.33	15	3.41	0.74
65	0.49	0.28	17	3.25	0.73
70	0.33	0.23	17	3.09	0.71
170	0.16	0.16	17	2.93	0.69
NE set (oldest), $N = 42$			20	2.76	0.67
3	6.83	1.05	20	2.60	0.65
5	6.66	1.04	20	2.44	0.63
5	6.50	1.03	23	2.28	0.61
6	6.34	1.01	24	2.11	0.59
7	6.18	1.00	25	1.95	0.56
7	6.01	0.99	25	1.79	0.54
7	5.85	0.98	27	1.63	0.51
7	5.69	0.96	30	1.46	0.49
7	5.53	0.95	30	1.30	0.46
10	5.36	0.93	32	1.14	0.43
10	5.20	0.92	35	0.98	0.40
10	5.04	0.90	38	0.81	0.36
12	4.88	0.89	40	0.65	0.33
12	4.71	0.88	40	0.49	0.28
12	4.55	0.86	57	0.33	0.23
13	4.39	0.84	70	0.16	0.16
13	4.23	0.83			

Table A2. Fault-length data (interpreted)

L (km)	ΣN^*	$\pm 1\,\sigma$	L (km)	ΣN^*	$\pm 1\,\sigma$
E–W set (youngest), $N = 67$			47	4.71	0.88
2	10.89	1.33	48	4.55	0.86
5	10.72	1.32	50	4.39	0.84
6	10.56	1.31	54	4.23	0.83
8	10.40	1.30	55	4.06	0.81
9	10.24	1.29	57	3.90	0.80
10	10.07	1.28	59	3.74	0.78
10	9.91	1.27	60	3.58	0.76
10	9.75	1.26	60	3.41	0.74
10	9.59	1.25	65	3.25	0.73
10	9.42	1.24	72	3.09	0.71
10	9.26	1.23	75	2.93	0.69
12	9.10	1.22	90	2.76	0.67
13	8.94	1.21	90	2.60	0.65
15	8.77	1.19	96	2.44	0.63
15	8.61	1.18	100	2.28	0.61
15	8.45	1.17	105	2.11	0.59
15	8.29	1.16	111	1.95	0.56
15	8.12	1.15	115	1.79	0.54
18	7.96	1.14	135	1.63	0.51
20	7.80	1.13	140	1.46	0.49
22	7.64	1.11	145	1.30	0.46
25	7.47	1.10	150	1.14	0.43
25	7.31	1.09	170	0.98	0.40
26	7.15	1.08	180	0.81	0.36
26	6.99	1.07	180	0.65	0.33
27	6.83	1.05	195	0.49	0.28
28	6.66	1.04	212	0.33	0.23
30	6.50	1.03	265	0.16	0.16
30	6.34	1.01	N–S set, $N = 54$		
35	6.18	1.00	2	8.77	1.19
35	6.01	0.99	3	8.61	1.18
35	5.85	0.98	3	8.45	1.17
35	5.69	0.96	4	8.29	1.16
36	5.53	0.95	4	8.12	1.15
37	5.36	0.93	6	7.96	1.14
40	5.20	0.92	6	7.80	1.13
40	5.04	0.90	8	7.64	1.11
45	4.88	0.89	10	7.47	1.10

Table A2. *Continued*

L (km)	ΣN^*	$\pm 1\,\sigma$	L (km)	ΣN^*	$\pm 1\,\sigma$
10	7.31	1.09	222	0.16	0.16
10	7.15	1.08	NE set (oldest), $N = 41$		
10	6.99	1.07	7	6.66	1.04
10	6.83	1.05	7	6.50	1.03
15	6.66	1.04	7	6.34	1.01
15	6.50	1.03	10	6.18	1.00
20	6.34	1.01	10	6.01	0.99
25	6.18	1.00	12	5.85	0.98
25	6.01	0.99	12	5.69	0.96
26	5.85	0.98	13	5.53	0.95
30	5.69	0.96	13	5.36	0.93
30	5.53	0.95	15	5.20	0.92
30	5.36	0.93	15	5.04	0.90
30	5.20	0.92	15	4.88	0.89
35	5.04	0.90	17	4.71	0.88
35	4.88	0.89	17	4.55	0.86
40	4.71	0.88	20	4.39	0.84
40	4.55	0.86	20	4.23	0.83
45	4.39	0.84	20	4.06	0.81
45	4.23	0.83	24	3.90	0.80
47	4.06	0.81	25	3.74	0.78
50	3.90	0.80	25	3.58	0.76
50	3.74	0.78	25	3.41	0.74
53	3.58	0.76	25	3.25	0.73
55	3.41	0.74	27	3.09	0.71
55	3.25	0.73	30	2.93	0.69
57	3.09	0.71	30	2.76	0.67
60	2.93	0.69	30	2.60	0.65
70	2.76	0.67	32	2.44	0.63
70	2.60	0.65	35	2.28	0.61
75	2.44	0.63	35	2.11	0.59
75	2.28	0.61	38	1.95	0.56
77	2.11	0.59	39	1.79	0.54
80	1.95	0.56	40	1.63	0.51
85	1.79	0.54	40	1.46	0.49
90	1.63	0.51	40	1.30	0.46
95	1.46	0.49	50	1.14	0.43
96	1.30	0.46	53	0.98	0.40
100	1.14	0.43	55	0.81	0.36
120	0.98	0.40	70	0.65	0.33
135	0.81	0.36	82	0.49	0.28
135	0.65	0.33	90	0.33	0.23
135	0.49	0.28	145	0.16	0.16
170	0.33	0.23			

N is the number of faults in the set having length L. N^* is normalized number of faults of given length per standard 10^4 km^2 reference area ($N^* = N \times 10^4/A$, where $A = 61{,}529$ km^2 is the area of plateau surface containing structures in the set). ΣN^* is cumulative normalized number of faults of given length. One standard deviation $\pm 1\,\sigma$ corresponds to statistical uncertainty relating number of faults to counting area A. $\sigma = \sqrt{\Sigma N^*(10^4/A)}$.